ACS Catalysis

Research Article

pubs.acs.org/acscatalysis

Highly Active Binder-Free Catalytic Coatings for Heterogeneous Catalysis and Electrocatalysis: Pd on Mesoporous Carbon and Its Application in Butadiene Hydrogenation and Hydrogen Evolution

Denis Bernsmeier,[†] Laemthong Chuenchom,[†,‡] Benjamin Paul,[†] Stefan Rümmler,[§] Bernd Smarsly,[‡] and Ralph Kraehnert*[,†]

[†]Department of Chemistry, Technische Universität Berlin, Straße des 17. Juni 124, 10623 Berlin, Germany

[‡]Institute of Physical Chemistry, Justus Liebig Universität, Heinrich-Buff-Ring 58, 35392 Giessen, Germany

[§]Institute of Chemistry, Martin-Luther-Universität Halle-Wittenberg, von-Danckelmann-Platz 4, 06120 Halle, Germany

Supporting Information

ABSTRACT: Heterogeneous catalysis performed in wall-coated reactors and electrocatalysis require homogeneous catalytic coatings with high surface area and good accessibility of the active sites. Conventional coating methods necessitate the use of binder components that often block pores and active sites, which limits catalytic efficiency, and utilization of expensive active metals. We report an approach for the direct and binder-free synthesis of chemically, mechanically, and thermally stable catalytic coatings based on ordered mesoporous carbon films employed as catalyst support. The synthesis relies on the codeposition of a structure-directing agent and small clusters of polymeric carbon precursors along with ionic metal species on a substrate. A sequence of thermal treatments converts the polymer into partly graphitized carbon, decomposes the structure-directing agent, and converts the metal precursor into highly active nanoparticles. Syntheses and catalytic applications are exemplarily demonstrated for palladium on carbon, a system widely used in heterogeneous catalysis and electrocatalysis. The obtained catalysts provide significantly higher space−time yields in the selective gas-phase hydrogenation of butadiene than all reported Pd/C catalysts while at the same time retaining isothermal reactor conditions. Moreover, when they were tested in the electrocatalytic hydrogen evolution reaction (HER), the catalysts outperformed reported Pd/C catalysts by a factor of 3, which underlines the benefits of the developed binder-free catalyst system.

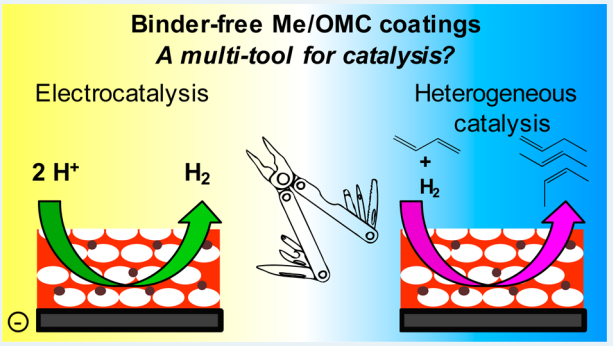

KEYWORDS: *catalyst synthesis, Nafion, carbon, palladium, HER, butadiene hydrogenation*

INTRODUCTION

Finely divided noble metals such as palladium are excellent catalysts for a wide range of chemical reactions. In heterogeneous catalysis supported Pd particles are employed, for example, in automotive catalytic converters[1] as well as numerous hydrogenation[2] and dehydrogenation[3] catalysts. In electrochemistry Pd catalyzes the hydrogen evolution reaction,[4] the oxygen reduction reaction,[5] and oxidation reactions.[6] Most of these catalysts use carbon as a support material due to its high abundance, stability, and electrical conductivity.[7]

Fast and highly exothermic Pd-catalyzed reactions in heterogeneous catalysis typically require the catalyst to be present in the form of a wall coating. Such coatings can transport the heat of reaction efficiently from the catalyst, thus avoiding hot-spot formation.[2c] Moreover, nanostructured porous coatings can provide a rapid mass transfer, which is required for efficient catalyst utilization.[8] Catalysts prepared on electrode plates in the form of surface coatings are also essentially required in electrocatalysis. These coatings need to ensure the rapid transport of electrons toward the active sites but should also provide good accessibility and short diffusion paths for electrolyte and product species.[9]

The most prominent technique to produce catalytic coatings for heterogeneous catalysis is so-called wash-coating.[10] Common synthesis methods employ a slurry prepared from fine-grained catalyst powders, a binder material, and a solvent for deposition of the coating. Typical oxide-based catalysts include micrometer-sized (Pt/Al_2O_3, Rh/Al_2O_3,[11] Al_2O_3[12]) or ball-milled (Al_2O_3,[13] $Pd/Na\text{-}Al\text{-}Si\text{-}O_x$[14]) powders of noble metals supported on oxides. Smaller sized particles are obtained from sols (Al_2O_3,[15,16] SiO_2,[15] TiO_2,[15] CeO_2[17]) with addition of active metal species prior to[16] or after deposition,[17] followed by calcination and reduction.

Received: August 5, 2016
Revised: October 24, 2016

© XXXX American Chemical Society

DOI: 10.1021/acscatal.6b02240
ACS Catal. 2016, 6, 8255−8263

Scheme 1. Illustration of the Synthesis Approach to Mesoporous Pd/OMC Catalyst Films[a]

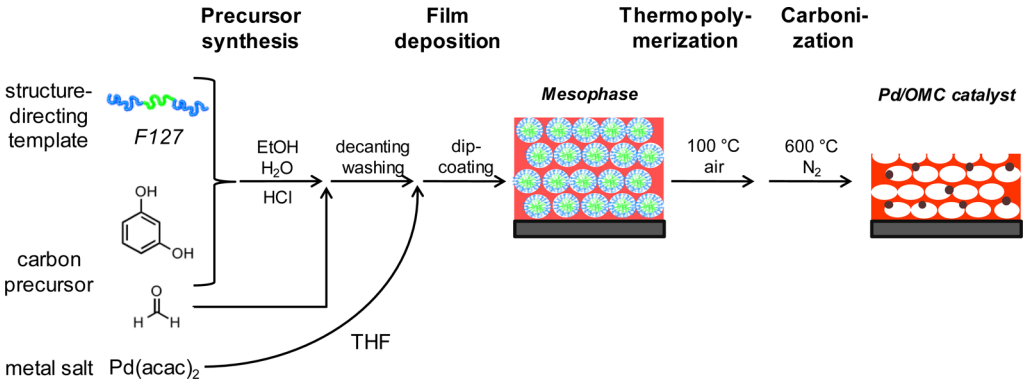

[a]The structure-directing triblock copolymer F127 (PEO-PPO-PEO) and resorcinol were dissolved in ethanol. After addition of hydrochloric acid, formaldehyde solution was added to start a polycondensation reaction. The derived polymeric resin was separated by centrifuging and washed. The polymeric compound was redissolved in a $Pd(acac)_2$-containing THF solution. Under controlled conditions a film was deposited via dip-coating to obtain a homogeneous mesophase film. After thermal treatment at 100 °C in air and a subsequent carbonization under an inert atmosphere (N_2) at 600 °C a mesoporous Pd/OMC film was obtained.

The most common method for the preparation of electrode coatings is the mixing of carbon-based catalyst powders and an ionomer binder (e.g., Nafion) with a solvent to form an ink. The ink is cast onto the electrode and dried. Unfortunately, binders such as Nafion can block pores and active sites and therefore degrade the coating performance.[18] Other challenges include the homogeneity of ink composition and coating, which critically influences the resulting electrical conductivity of the deposited film and makes the accurate and reproducible synthesis of electrode coatings rather challenging.[19]

Binder-free coatings of carbon have been reported in the form of so-called "ordered mesoporous carbon" (OMC), a carbon material with templated mesoporosity which is accessible via soft templating with micelles of block copolymers.[20] Parameters such as porosity and degree of graphitization can be finely tuned.[21] Furthermore, heteroatom doping of the carbon network and surface modifications are accessible.[20,22] OMC films combine a number of properties desired in catalysis: i.e., high surface area, tunable pore size, high porosity, chemical inertness, and electrical conductivity.[9,23] These attributes make OMC films ideal candidates as catalyst support materials for electrodes, membranes, and wall-coated reactors in heterogeneous catalysis. However, suitable ways of introducing active sites such as particles of noble metals are required.

Common methods for the synthesis of films of ordered mesoporous carbon employ micelles of amphiphilic molecules deposited along with small clusters of a polymeric resin.[24] Interactions between the thermoplastic resin and a thermally decomposable copolymer during evaporation-induced self-assembly (EISA) result in formation of an ordered nanocomposite film. Subsequent heat treatments stabilize the polymeric framework, decompose the template molecules, and finally transform the remaining polymer into a porous carbon material.[9] A variety of precursors, solvents, and structure-directing agents can be used from the film synthesis. Dai and co-workers[25] synthesized a hexagonally ordered mesoporous film employing PS-P4VP as a template. Tanaka et al. reported hexagonally ordered carbon films (COU-1) using Pluronic F127 (PEO-*b*-PPO-*b*-PEO) as template.[26] Other templates include Brij58[23a] and Pluronic P123.[27] Resorcinol,[25,26,28] phloroglucinol,[29] phenol,[27,30] and 1,5-dihydroxynaphthalene[23c] together with formaldehyde[23b,31] can be used as precursors.

The synthesis of templated OMC films has at least three basic requirements,[24] all of which could be significantly influenced by the additional presence of metal species. (1) The template polymer needs to assemble with the precursor clusters to form an ordered mesophase. (2) The template needs to decompose at a temperature lower than that for the cross-linked precursor. (3) The formed pore structure needs to be retained despite a massive loss of volatile species[25] and contraction of the system[32] during the final pyrolysis step. A catalytically active metal could be incorporated into the film synthesis in two different ways, either as a dissolved metal salt or as preformed metal nanoparticles dispersed in the solution that is used for film casting. Major challenges result from a severe aggregation and sintering of dissolved metal species during carbonization (>600 °C), which produces large particles and a broad size distribution.[33] Moreover, stabilizing agents that protect colloidal metal particles from aggregation often also prevent the self-assembly of the polymeric precursor and pore template.[33] In addition, the interaction between metal and carbon species during carbonization and pore formation remains so far largely unexplored. A direct synthesis of catalytically active noble-metal-containing OMC films has therefore not been reported so far.

We report the first direct synthesis route to mechanically, chemically, and thermally stable OMC films that incorporate exemplarily catalytically active palladium particles. The general synthesis procedure is illustrated in Scheme 1. The synthesis is based on the redissolution of a prepolymerized RF resin that already contains a structure-directing agent (Pluronic F127) in THF along with dissolved metal precursors. The use of metal salts that are soluble in THF is a key requirement of the synthesis. After film deposition of the combined solution via dip-coating, thermal cross-linking, and carbonization, an electrically conductive mesoporous carbon film is obtained that contains small and accessible metal particles.

The following sections present the synthesis details and the obtained morphology, crystallinity, and porosity of carbonized Pd/OMC film as well as its catalytic activity studied exemplarily in heterogeneous catalysis (butadiene hydrogenation) and electrocatalysis (hydrogen evolution reaction (HER)). The

DOI: 10.1021/acscatal.6b02240
ACS Catal. 2016, 6, 8255−8263

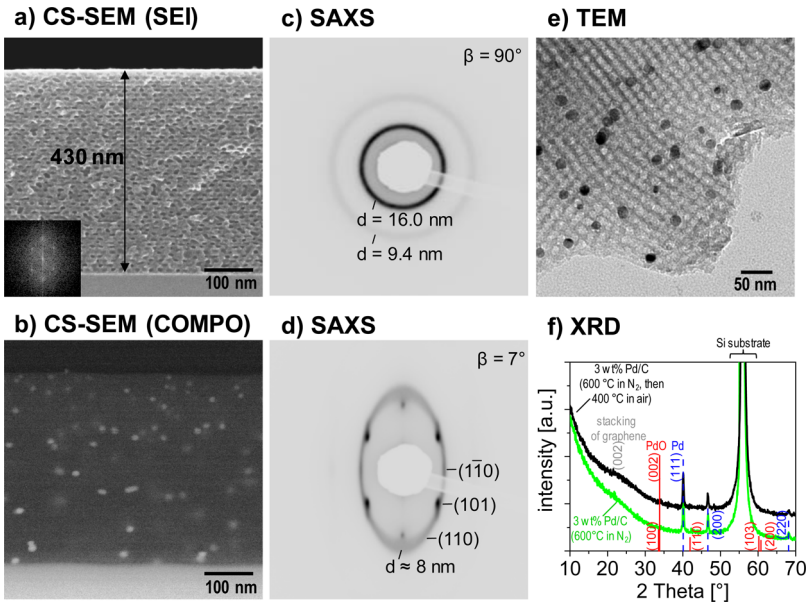

Figure 1. Physicochemical analysis of a F127-templated ordered mesoporous carbon film, containing 3 wt % Pd, carbonized at 600 °C. Cross-section SEM image in secondary electron mode with FFT inset (a) and in backscattered electron mode (b). 2D-SAXS patterns with incident angles of β = 90° (c) and β = 7° (d). The anisotropic ring in (c) can be attributed to regular pore lattice distances of 16.0 nm in first order and 9.4 nm in second order. The scattering spots in (d) are indexed according to a face-centered-cubic pore lattice (space group $Im\bar{3}m$) with (110) orientation in respect to the substrate surface. TEM micrograph of a scraped off film segment (e) showing homogeneously distributed PdNP (dark spots) in an ordered mesoporous carbon matrix. XRD analysis (f) of a film carbonized at 600 °C in comparison to a film additionally treated at 400 °C in air. Assigned (*hkl*) indices correspond to cubic Pd metal (PDF 46-1043) and cubic PdO (PDF 41-1107). A broad reflection (24°) can be attributed to stacking of graphene.[35]

comparison to conventional catalysts reported in the literature illustrates the superior performance of the binder-free Pd/OMC in both types of applications.

RESULTS AND DISCUSSION

Physicochemical properties of Pd/OMC Films. Figure 1 presents for a typical Pd/OMC catalyst film carbonized for 3 h at 600 °C in nitrogen flow SEM cross-section images in (a) secondary electron mode and (b) backscattered electron mode, 2D-SAXS patterns recorded with incident angles of (c) β = 90° and (d) β = 7°, (e) a TEM micrograph of a film segment, and (f) diffraction patterns obtained by XRD. The film contains 3 wt % Pd (from WDX analysis and StrataGem evaluation).[34]

The SEM cross-section image (Figure 1a) recorded in secondary electron image mode indicates that the Pd/OMC films exhibit a homogeneous and locally ordered pore structure throughout the film without cracks, aggregates, or other irregularities. The film thickness amounts to ca. 430 nm. The templated mesopores feature dimensions of 8 nm parallel and 6 nm perpendicular to the substrate. The FFT obtained from the SEM image (inset in Figure 1a) features an ellipsoidal pattern with bright spots that can be attributed to periodic pore distances of 14 nm parallel and 9 nm perpendicular to the substrate. The diffraction spots can be assigned to the (110) and (101) planes of a cubic closed packing of pores and therefore indicate a high degree of ordering. The ellipsoidal pore shape originates from a uniaxial film contraction during template removal, which is in line with the ellipsoidal nature of the pores.[8b]

SEM images recorded with backscattered electrons on the same film position (Figure 1b) indicate the location of Pd-containing particles as bright spots caused by higher metal *z* contrast. The formed Pd particles appear to be separate and distributed throughout the whole volume of the mesoporous carbon film.

N_2 sorption analysis of a corresponding Pd/OMC powder sample confirms a narrow size distribution of the formed mesopores around 5 nm (see QS-DFT evaluation of a full N_2 isotherm, Figure S3 in the Supporting Information). This observation is consistent with the pore sizes observed from SEM images. The deduced total pore volume amounts to 0.46 cm^3/g. A total of 40% of this pore volume can be assigned to micropores. The accessible surface area of a Pd/OMC film carbonized at 600 °C was obtained via BET analysis of a Kr physisorption measurement and amounts to 590 m^2 per cm^3 film volume.

Small angle X-ray scattering (SAXS) patterns of Pd/OMC films carbonized at 600 °C show a high degree of pore ordering (Figure 1c,d). The pattern recorded at 90° beam incident angle with respect to the film surface plane shows two isotropic rings that can be attributed to *d* spacing values of 16.0 and 9.4 nm of the mesopore lattice (Figure 1c). SAXS measured in gracing incidence (Figure 1d) shows an ellipsoidal shape that indicates uniaxial film shrinkage perpendicular to the substrate. The bright scattering spots can be assigned to the lattice planes (1$\bar{1}$0) as well as (101) of a contracted cubic pore system.[36] The *d* spacing value perpendicular to the substrate amounts to 8 nm, which indicates a film contraction of ca. 50% during template removal and carbonization. Comparing Pd/OMC catalysts containing 3 wt % Pd to Pd-free OCM samples indicates that the added metal does not have a significant influence on the obtained degree of pore ordering. However, additional tests with platinum concentrations exceeding 3 wt % Pt suggest that for high metal loadings a lower degree of pore ordering can be expected.

DOI: 10.1021/acscatal.6b02240
ACS Catal. 2016, 6, 8255−8263

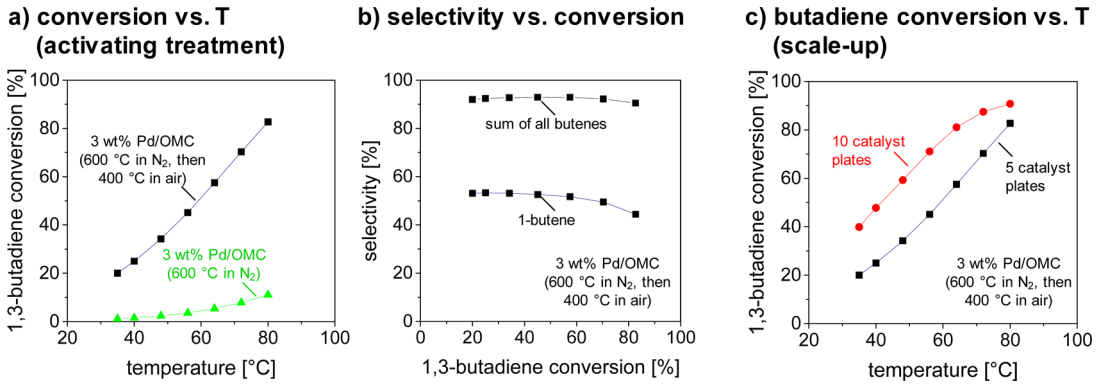

Figure 2. Catalytic performance of mesoporous Pd/OMC catalytic coatings in the selective gas-phase hydrogenation reaction of 1,3-butadiene. (a) Butadiene conversion vs temperature. The Pd/OMC catalyst with 3 wt % Pd loading treated for 5 min at 400 °C in air is compared to a nontreated Pd/OMC catalyst. (b) Selectivity to 1-butene and total butene selectivity vs butadiene conversion. (c) Butadiene conversion vs temperature of 5 coated catalyst plates compared to a scaled-up approach with 10 plates. Both catalyst sets were pretreated for 5 min at 400 °C in air. The reaction feed contained 5% butadiene and 10% hydrogen in nitrogen at a constant flow rate of 30 mL/min. The composition of the product gas flow was studied at seven different temperatures between 35 and 80 °C.

A TEM micrograph of a Pd/OMC film segment (Figure 1e) confirms the homogeneous distribution of Pd particles and a particle size of about 14.3 ± 3.2 nm with particles being located inside a well-ordered mesoporous carbon framework. The majority of the particles located inside the film remain small. XRD patterns (Figure 1f) were obtained for Pd/OMC films carbonized at 600 °C in nitrogen and for films treated additionally for 15 min at 400 °C in air in order to remove carbon species from the surface of Pd particles (see also Figure S4 in the Supporting Information). Clear reflections can be observed at 40.1, 46.7, and 68.1°, which correspond well with the (111), (200), and (220) lattice planes of metallic palladium (PDF 46-1043). SAED analysis (not shown) confirms that Pd is present in a metallic state. The XRD signal at 56° results from the substrate (Si wafer) employed for the Pd/OMC film samples studied in XRD. Reflections corresponding to palladium oxide were not observed, indicating that no Pd bulk oxide phase is formed. The crystallite size estimated via the Scherrer equation amounts to ca. 26 nm. A broad reflection around 24° can be attributed to the (002) lattice plane of disordered small graphene stacks.[35]

XP spectra were recorded in the Pd_{3d} and C_{1s} region in order to assess the near-surface composition of the material (Figure S5 in the Supporting Information). The Pd_{3d} spectrum (Figure S5a) is dominated by a signal that corresponds to metallic Pd (335.0 eV)[37] and smaller contributions of PdO and PdO_2 at 336.2 eV[38] and 337.6 eV,[39] respectively. The oxide contributions are attributed to a surface oxidation of Pd when the film sample is exposed to ambient air during sample transfer and storage. An intense peak in the C_{1s} region (Figure S5b) confirms the dominating presence of graphitic carbon.[40]

Partial graphitization is an essential requirement of the film synthesis in order to produce materials with an electrical conductivity high enough to allow electrocatalytic reactions to occur on the formed Pd particles. The electrical conductivity measured for Pd/OMC films carbonized at 600 °C amounts to 0.03 S/cm. Adhesion of a Pd/OMC film to a steel substrate was tested by the tape test.[41] As depicted in Figure S1 in the Supporting Information, no carbon film was peeled off after pulling off a tape. This behavior indicates good mechanical stability and strong adhesion of the carbon film to the substrate.

The developed synthesis approach thus produces conductive carbon films with well-ordered mesopores throughout the film volume with a high surface area. The formed metallic Pd nanoparticles are well dispersed, and the presence of Pd does not disturb the formation of the open-porous carbon network. The carbon shows a small degree of graphitization and good electrical conductivity.

Catalytic Performance in Butadiene Hydrogenation. The developed Pd/OMC catalytic coatings were tested in a microstructured reactor designed to accommodate 5 and 10 catalyst plates with minimal channel width (1625 and 830 μm, respectively). The reactor design (see Figure S2b in the Supporting Information) maximizes the contact area between the catalytic coating and thermally conductive reactor material to ensure that very fast and exothermic reactions such as the hydrogenation of butadiene can be studied under isothermal conditions.

Figure 2 displays catalytic results obtained with a stack containing five reactor plates coated on both sides with Pd/OMC, carbonized at 600 °C under an N_2 atmosphere, and additionally treated for 5 min at 400 °C in air to remove carbon species. Shown are (a) butadiene conversion vs temperature with and without the initial air treatment, (b) selectivity vs conversion, and (c) a comparison of butadiene conversion between reactors comprising five and ten stacked catalyst plates.

Figure 2a indicates a poor activity for the film treated only in N_2, with a butadiene conversion reaching less than 11% at 80 °C. After additional treatment of a corresponding Pd/OMC film in air (5 min, 400 °C) a drastically higher activity can be observed that reaches 20% already at 35 °C and 83% at 80 °C. The strongly enhanced performance suggests that the Pd particles contained in the "as carbonized" Pd/OMC film might be covered by a thin carbon shell, which can be removed by the air treatment and results in a highly active hydrogenation catalyst (see Figure S4 in the Supporting Information for more information).

Figure 2b plots for the air-treated Pd/OMC catalyst the selectivity toward 1-butene and toward the sum of all butenes vs the butadiene conversion. The catalyst performs very selectively. At low conversion selectivities amount to about 54% (1-butene) and 92% (sum of all butenes). The observed 1-butene selectivity agrees well with typical Pd/C and Pd/TiO_2 catalysts reported in the literature.[8b,34,42] More remarkably, the high selectivity to 1-butene is retained also well above 80%

DOI: 10.1021/acscatal.6b02240
ACS Catal. 2016, 6, 8255−8263

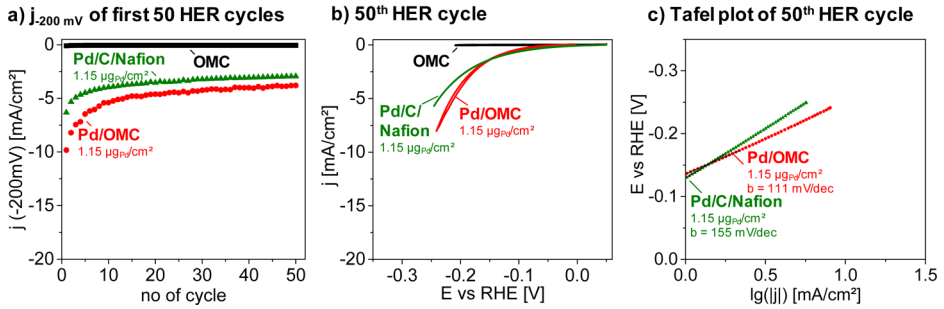

Figure 3. Electrocatalytic performance of Pd/OMC, Pd/C/Nafion, and Pd-free OMC films in the HER: (a) current response at a potential of −200 mV (vs RHE) plotted vs cycle number derived from the first 50 cathodic sweeps during CV testing; (b) geometric current density plotted vs potential for the 50th cycle of CV testing; (c) Tafel evaluation (potential vs log(current density) for the 50th cycle. The first 15 points in the HER regime were employed for linear fitting. All CVs were recorded in 0.5 M sulfuric acid with a scan rate of 20 mV/s. The graphs compare a mesoporous 3 wt % Pd/OMC catalyst with a Pd-free OMC coating (390 nm thick film) and a conventional Pd/C/Nafion reference catalyst film based on a Nafion ink and commercial Pd/C (5 wt % on activated carbon). Both Pd-containing catalysts feature the same geometric Pd loading of 1.15 $\mu g_{Pd}/cm^2$.

butadiene conversion, whereas typical catalysts reported in the literature show a significant decrease in selectivity starting already at butadiene conversion levels of about 50% (Pd/TiO_2 in ref 2c) to 60% (Pd/C in ref 42b, Pd/TiO_2 in refs 8b and 42a).

The space−time yield of butene formed per mass of Pd contained in the catalyst can be used to compare the performance of different reported Pd/C catalysts directly. Yan et al.[42b] reported performance data obtained under conditions comparable to those of our study (48 °C, c_{H2}:c_{BD} = 2.5:1, 110 μg of active Pd, 1.01 bar). The reported catalysts include a commercial Pd/C, Pd nanoparticles supported on graphene, and single-site Pd catalysts supported on graphene. The obtained STYs for those catalysts amount to 2.5, 2.5, and 3.0 $mol_{butene}\ s^{-1}\ kg_{Pd}^{-1}$, respectively. In contrast, the Pd/OMC catalyst presented in Figure 2a produces 3.8 $mol_{butene}\ s^{-1}\ kg_{Pd}^{-1}$, which indicates a 25−50% higher mass-specific catalytic activity toward butene formation.

Different factors might be contributing to the observed high activity. Silvestre et al. and Dal Santo et al. reported that butadiene hydrogenation is a highly structure sensitive reaction.[43] The hydrogenation reaction occurs on the Pd (111) surface sites for supported Pd particles that exceed a particle size of 4 nm.[43a] A closer look at the shape of the particles in this work reveals that the predominant particle shape is octahedral with some minor fractions of truncated octahedra. The facets of octahedra are (111). Thus, hydrogenation on (111) surfaces is likely to be the dominating reaction. Moreover, Schauermann, Freund, and co-workers reported in a series of publications that the presence of subsurface carbon atoms on Pd surfaces drastically lowers the activation barrier for subsurface migration of H atoms on Pd (111) facets, which critically influenced the corresponding activity and selectivity of olefin conversions in their studies.[44] During the high-temperature treatment of our Pd/OMC catalysts, carbon species were abundantly present, which makes the migration of carbon into the subsurface region of Pd particles likely and could explain the high hydrogenation reactivity. However, such subsurface carbon species are very difficult to analyze and thus are beyond the scope of this work.

Further insights can be gained from the Arrhenius plots. The activation energy derived for Pd/OMC between 35 and 56 °C amounts to 31.5 kJ/mol. This value is about 50% lower than activation energies reported for oxide-supported Pd catalysts (Pd/TiO_2, 68 kJ/mol[45] and 62 kJ/mol;[8b,42a] Pd/Al_2O_3, 48−66 kJ/mol[2d]) as well as carbon-supported Pd (Pd/C, 58 kJ/mol; PdNP/graphene, 65 kJ/mol; both calculated from data reported in ref 42b). An apparent energy of activation which amounts to about half the value of the true activation energy is a typical indicator of transport limitations by pore diffusion.[46] Physisorption measurements on the Pd/OMC catalysts indicate that about 40% of their total pore volume can be assigned to micropores (see Figure S3 in the Supporting Information). The observed apparent energy of activation of 31.5 kJ/mol could thus indicate that a major fraction of the active Pd could be located inside micropores. However, Pd/OMC still outperforms all comparable carbon-supported Pd catalysts reported in the literature in terms of butene formation rates.

One specific advantage of the developed synthesis route is the simple and facile scale-up of the catalyst and reactor production via "numbering up" of the number of catalyst plates fitted into the reactor housing. A photo of a microstructured reactor fitted with 5 and 10 catalyst plates is shown in Figure S2 in the Supporting Information. The corresponding performance of both catalyst stacks is compared in Figure 2c in terms of butadiene conversion plotted vs temperature. At 35 °C the conversion amounts to 20% (five plates) and 40% (10 plates): i.e., twice as high. Moreover, the observed space−time yield amounts to 2.2 $mol_{butene}\ s^{-1}\ kg_{Pd}^{-1}$ for both configurations, illustrating perfect scale-up behavior. The data illustrate the simplicity of the scale-up of catalyst and reactor and confirms that excellent temperature control and close to isothermal conditions can be retained despite the doubled amount of heat produced by the fast and highly exothermic reaction.

Electrocatalytic Performance in the Hydrogen Evolution Reaction. The HER performance of Pd/OMC catalyst films deposited on glassy carbon was tested by cyclic voltammetry (CV) performed in acidic medium (0.5 M H_2SO_4). The catalyst films were carbonized at 600 °C and then treated for 5 min at 400 °C in air (oxidative cleaning) and 15 min in H_2/Ar atmosphere at 400 °C (reduction). Figure 3 plots (a) the current density recorded at −200 mV during the first 50 cycles, (b) the 50th recorded CVs as current density vs applied potential, and (c) the corresponding Tafel plots for the Pd/OMC catalyst as well as a conventional Pd/C/Nafion catalyst shown for reference. Both catalysts feature the same Pd loading (1.15 $\mu g/cm^2$). Figure 3b shows in addition the activity of Pd-free OMC.

DOI: 10.1021/acscatal.6b02240
ACS Catal. 2016, 6, 8255−8263

Table 1. Comparison of the HER Performance in Acidic Solution of the Herein Presented Catalysts Pd/OMC and Pd/C/Nafion with State of the Art Catalysts Reported in the Literature

author	catalyst	Pd loading (μg/cm^2)	electrolyte	j at −200 mV (mA/cm^2)	$j_{mass\text{-}based}$ at −200 mV (mA/μg_{Pd})	Tafel slope b (mV/dec)
this study	Pd/OMC	1.15	0.5 M H_2SO_4 (N_2)	−3.7	−3.2	111
this study	Pd/C/Nafion	1.15	0.5 M H_2SO_4 (N_2)	−2.9	−2.5	155
Bhowmik et al.[49]	Pd/C/Nafion	43	0.5 M H_2SO_4 (N_2)	−16	−0.37	121
Bai et al.[50]	PdNP/Nafion	46	0.5 M H_2SO_4 (Ar)	−11	−0.24	85
Bai et al.[50]	PdNP/rGO/Nafion	46	0.5 M H_2SO_4 (Ar)	−50	−1.1	
Pentland et al.[48]	pc Pd[a]		0.01 M HCl			107

Pd/OMC shows throughout the first 50 cycles a significantly higher HER current than the Pd/C/Nafion reference coating (Figure 3a). Moreover, both catalysts show decreasing currents in the first 20 cycles followed by a regime of stable performance. The initial activity follows a similar pattern for both catalysts and is therefore not specific to Pd/OMC. The decrease could be related to an initial saturation of the electrolyte with the formed hydrogen gas that hinders subsequent hydrogen desorption.

The CVs depicted in Figure 3b for the 50th cycle indicate the HER activity as a function of potential. No oxidation or reduction features other than HER are observed. Both Pd/OMC and Pd/C/Nafion contain the same amount of Pd. The Nafion-free Pd/OMC catalysts show higher HER currents particularly at a more negative applied potential: i.e., higher current densities. Ordered mesoporous carbon films without palladium (Figure 3b "OMC") show no signs of HER activity or any other reductive currents.

Tafel evaluation plots can provide insights into mechanistic aspects and transport limitations in the HER.[47] Figure 3c displays Tafel plots for Pd/OMC and Pd/C/Nafion after 50 HER cycles. The observed Tafel slopes amount to 111 mV/dec for Pd/OMC and 155 mV/dec for Pd/C/Nafion. Pentland et al. derived a Tafel slope of about 99−107 mV/dec for unsupported polycrystalline Pd.[48] Bhowmik et al. reported similar values around 121 mV/dec for Pd/C/Nafion catalysts.[49] Bai et al. observed 85 mV/dec for preformed Pd cubes (d = 10 nm) fixed with Nafion on a working electrode.[50] Hence, Pd/OMC exhibits Tafel slope values that are well within the range of literature values reported for Pd. Values around 120 mV/dec were reported to be indicative for the discharge of a proton on the metal surface to be rate determining (Volmer reaction: $H^+ + e^- + M \rightleftharpoons MH_{ads}$).[47]

The intrinsic activity of different Pd-based catalysts can be compared on the basis of the mass-normalized current density recorded at the same overpotential. Table 1 compares for different catalysts the current density measured at −200 mV vs RHE, the corresponding Pd loading, the mass-normalized activity, and the respective reported Tafel slopes. The new Pd/OMC catalysts achieve a mass-normalized HER current of −3.2 mA per μg Pd after 100 cycles, whereas the Pd/C/Nafion measured for comparison reaches only −2.5 mA/μg_{Pd}. Carbon-supported catalysts reported in the literature show lower activities in general. Bhowmik et al. report −0.37 mA/μg_{Pd} for a Pd/C/Nafion catalyst.[49] Catalysts reported by Bai et al. perform with −0.24 mA/μg_{Pd} (Pd nanocubes/Nafion) and −1.15 mA/μg_{Pd} (Pd nanocubes/reduced graphene oxide (rGO)/Nafion).[50] Hence, the Nafion-free Pd/OMC catalysts outperform the Pd/carbon catalysts reported in the literature by at least a factor of 3.

CONCLUSION

Highly active binder-free carbon-based supported catalysts can be synthesized in the form of wall coatings by a synthesis route that employs the codeposition of a structure-directing agent and small clusters of polymeric carbon precursors along with ionic metal species on a substrate. A sequence of thermal treatments converts the polymer into partly graphitized carbon, decomposes the structure-directing agent, and converts the metal precursor into highly active nanoparticles. The resulting Pd/OMC films contain small Pd particles well distributed in a mesoporous carbon matrix with high surface area, chemical, mechanical, and thermal stability, and electrical conductivity. The presented concept omits the necessity of a binder (e.g., Nafion) in the synthesis of the catalytic coating.

The binder-free Pd/OMC films prove to be highly active in the gas-phase hydrogenation of butadiene as well as the electrocatalytic hydrogen evolution reaction. In butadiene hydrogenation the obtained Pd/OMC coatings provide significantly higher space−time yields than all reported Pd/C catalysts while at the same time enabling isothermal reactor conditions. The presented concept provides an easy path for the scale-up of synthesis and reaction while preserving ideal operating conditions. Moreover, when tested in the electrocatalytic hydrogen evolution reaction (HER), the catalysts outperform reported Pd/C catalysts by a factor of 3, which underlines the benefits of the developed binder-free catalyst system.

The presented concept paves the way to the controlled synthesis of a wide range of highly active catalytic coatings that employ carbon as a support for other active metals such as Pt, Ru, and Rh and the opportunity to study these catalysts under very defined reaction conditions. Moreover, the catalyst properties can be easily tuned and enable the investigation of parameters such as pore size, film thickness, and conductivity, and in particular of the role of Nafion in electrocatalysis.

EXPERIMENTAL SECTION

Chemicals. Resorcinol, formaldehyde (37 wt % in water), and Pluronic F127 (PEO_{106}-b-PPO_{70}-b-PEO_{106}, M_w = 12600) were purchased from Sigma-Aldrich. Milli-Q water was used for all synthesis procedures. Ethanol (EtOH, >99.9%, absolute) and tetrahydrofuran (THF, >99.9%, absolute) were purchased from VWR. Hydrochloric acid (HCl, 3 M) was prepared from 12 M HCl (Alfa Aesar). Palladium(II) acetylacetonate ($Pd(C_5H_7O_2)_2$ or $Pd(acac)_2$, 98%) was purchased from Alfa Aesar. A 5% Nafion solution, isopropyl alcohol, and Pd on activated carbon (Cat. No. 20.568-0, 5 wt %) were obtained from Sigma-Aldrich. All chemicals were used without further purification.

Substrate Pretreatment. Si wafer substrates were cleaned with ethanol and calcined in air (2 h, 600 °C) prior to film

DOI: 10.1021/acscatal.6b02240
ACS Catal. 2016, 6, 8255−8263

deposition. Stainless steel plates (1.4301) were cut into 33 × 27 mm substrates. The steel substrates were ground, washed, and calcined as described earlier.[8b] Glassy-carbon (Sigradur G) substrates were purchased from HTW. All glassy-carbon (GC) substrates were polished with a 0.05 μm diamond dispersion and cleaned thoroughly with ethanol and water. SiO_2 glass substrates for conductivity measurements were purchased from UniversityWafer and cleaned with ethanol.

Synthesis of Pd/OMC: Pd-Containing Mesoporous Carbon Films and Powders. For the catalyst synthesis according to Scheme 1 a 1.1 g amount of of resorcinol was mixed with 0.3 g of F127 in 4.5 mL of EtOH until a clear solution was obtained. Then 4.5 mL of 3 M HCl was added. The mixture was stirred for 5 min. A 1.3 g portion of formaldehyde (37% in water) was added and thoroughly mixed. After ca. 4 min the solution became turbid. Ten minutes after the addition of the formaldehyde solution, a white precipitate was separated from the mixture by centrifugation at 7500 rpm for 5 min and the top-layer solution was discarded. The white precipitate was washed with water and then dissolved in 5 mL of THF containing 31.5 mg of dissolved $Pd(acac)_2$. A clear orange dispersion was obtained and used for dip-coating. Films were deposited via dip-coating at 25 °C and 30% relative humidity. The coated substrates were thermally treated at 100 °C for 12 h in air, followed by carbonization at 600 °C for 3 h under a flowing nitrogen atmosphere (heating ramp of 1 K/min). The corresponding powder samples were prepared by drying the dip-coating suspension in a crucible followed by an thermal treatment identical with that applied to the films. For enhanced catalytic performance, films were additionally treated in a muffle furnace at 400 °C for 5 min in air to remove residual carbon from the formed Pd particles. In case of electrocatalytic testing in the hydrogen evolution reaction the catalyst was in addition treated for 15 min at 400 °C in a tube furnace under an atmosphere of 5% hydrogen in argon.

Synthesis of Pd/C/Nafion Reference Catalyst. The reference catalyst was prepared by dissolving 5 mg of Pd/active carbon (5 wt %) in 3.98 mL of water. A 20 μL portion of Nafion solution (5%) was carefully added. After addition of 1 mL of isopropyl alcohol the mixture was sonicated for 15 min with 6 W output power with a Branson Sonifier. The resulting ink was immediately employed for film deposition via drop-casting and subsequent drying at 60 °C. The resulting reference catalyst film had a geometric Pd loading of 1.15 $\mu g/cm^2$. In the following the catalyst will be denoted as Pd/C/Nafion.

Physicochemical Properties. SEM images were collected on a JEOL 7401F instrument at 10 kV. The ImageJ program, version 1.39u (http://rsbweb.nih.gov/ij), was employed to determine the pore diameter, film thickness, and size of Pd particles and to obtain fast Fourier transformed (FFT) images. TEM and selected area electron diffraction (SAED) images were recorded on a FEI Tecnai G^2 20 S-TWIN instrument operated at 200 kV on fragments of film samples scraped off the substrates and deposited on carbon-coated copper grids. To determine the amount of the Pd in the film, the mass depth was calculated using the STRATAGem film analysis software (v 4.8) on the basis of wavelength dispersive X-ray (WDX) spectra analyzed with a JEOL JXA-8530F electron microprobe at 7 and at 10 kV.

Films coated on thin silicon wafers (50 μm) were used for 2D-SAXS measurements. 2D-SAXS patterns were collected at the μSpot beamline at the BESSY II synchrotron (Berlin, Germany) with a calibrated radiation energy of 12.399 keV. The SAXS data were processed employing the software FIT2D Version V12.077. XRD was measured on a Bruker D8 Advance instrument (Cu Kα radiation) with a gracing incident beam (1°). XP spectra were recorded with an Omicron DAR 400 X-ray source with Al Kα excitation. Electrons were detected with an EA 125X Hemispherical Energy Analyzer.

Two-point sheet conductivity measurements were performed with a Keithley Model 6517B Electrometer employing a 8 × 8 pin probe head with an altering polarity sequence of the pins. Kr and N_2 adsorption isotherms were measured at 77 K with a Quantachrome Autosorb-iQ instrument. The samples were degassed under vacuum at 150 °C for 2 h prior to sorption analysis. The surface areas were determined by the Brunauer–Emmett–Teller (BET) method. Pore size evaluation was done with a QSDFT equilibrium Kernel and a model assuming cylindrical pores.

Adhesion of a carbonized Pd/OMC coating to a steel substrate was tested by the "tape test" as described in ASTM D3359 *Standard Test Methods for Measuring Adhesion by Tape Test* (http://www.astm.org/Standards/D3359.htm). An X-cut was made through the coating penetrating the substrate. An adhesive tape (Scotch tape) was applied over the cut. The tape was smoothed and then pulled away. Poorly adhered coatings would peel away with the tape, whereas well-adhered coatings would be stable. Photographs before and after the test were taken, employing an Olympus BX40 optical microscope.

Catalytic Testing in Hydrogenation of 1,3-Butadiene. Pd/OMC films were coated on both sides of steel substrates. For each catalytic run, 5 or 10 identical steel plates with the same thickness (0.5 mm for 5 plates and 0.25 mm for 10 plates) were stacked parallel into the reactor housing. Photographs of a catalyst stack and the reactor are presented in Figure S2 in the Supporting Information. A test setup and procedure similar to that described in refs 8b and 51 was used. A reaction mixture consisting of 5% butadiene (2.5 purity), 10% hydrogen (5.0 purity), and 85% nitrogen (5.0 purity) was passed through the reactor at a flow rate of 60 mL/min (STP) at 1.05 bar. The catalyst was heated to 80 °C under a reactive gas flow and equilibrated to reaction conditions for several hours. Afterward, the temperature was gradually decreased stepwise from 80, 72, 64, 56, 48, and 40 °C and finally to 35 °C with a dwell time of 60 min for each temperature set point. Analysis of the gas products was continuously performed every 7 min by an online gas chromatograph (Agilent GC 7890 equipped with FID, TCD, and columns HP Plot Al_2O_3, Molsieve 5A, HP Plot Q, and DB FFAP). The space–time yield (STY) was calculated as moles of butenes produced per second per kilogram of the catalyst ($mol_{butene}\ s^{-1}\ kg_{catalyst}^{-1}$) and kilograms contained ($mol_{butene}\ s^{-1}\ kg_{Pd}^{-1}$).

Electrocatalytic Testing in Hydrogen Evolution Reaction in Acidic Medium. All electrocatalytic testing was performed by using a three-electrode disk setup with a RHE (Gaskatel, HydroFlex) as a reference and Pt gauze (ChemPur, 1024 mesh cm^{-2}, 0.06 mm wire diameter, 99.9%) as a counter electrode. All potentials in this work are referenced to the reversible hydrogen electrode. Small disks with a diameter of 6 mm were cut out from the coated GC substrates. These homogeneously coated disks were mounted on a rotating disk shaft and served as working electrodes (n = 2000 rpm) using 0.5 M H_2SO_4 as the supporting electrolyte (Fixanal, Fluka Analytical) and a BioLogic SP-200 instrument as the potentiostat. The electrolyte solution was purged for at least 30 min with nitrogen before the catalytic tests. Prior to testing a

DOI: 10.1021/acscatal.6b02240
ACS Catal. 2016, 6, 8255–8263

break-in procedure was conducted (50 potential cycles) in the cathodic regime (50 to −210 mV) followed by a conditioning time of 2 h at open circuit potential. During break-in treatment and in the subsequent HER measurement a flow of N_2 gas was maintained over the electrolyte. The activity in the hydrogen evolution reaction was investigated by cyclic voltammetry (50 cycles) in a potential window of 50 to −210 mV vs RHE with a scan rate of 20 mV s^{-1}.

■ ASSOCIATED CONTENT

Supporting Information

The Supporting Information is available free of charge on the ACS Publications website at DOI: 10.1021/acscatal.6b02240.

Photographs of the film adhesion test and reactor design as well as additional physicochemical characterization via SEM, N_2 sorption, and XPS (PDF)

■ AUTHOR INFORMATION

Corresponding Author

*E-mail for R.K.: ralph.kraehnert@tu-berlin.de.

Notes

The authors declare no competing financial interest.

■ ACKNOWLEDGMENTS

The authors thank Björn Eckhardt, Katrin Schulz, Roman Schmack, and Arno Bergmann from TU Berlin, Eik Koslowski from Universität Halle, and Sören Selve and Jörg Nissen from the ZELMI (TU Berlin) for support in material analytics. We acknowledge funding from the BMBF (FKZ 03EK3009). R.K. thanks in particular the Einstein Foundation Berlin for generous support provided by an Einstein-Junior-Fellowship (EJF-2011-95). SAXS measurements were conducted at the μSpot beamline at the BESSY II synchrotron.

■ REFERENCES

(1) Bonet, F.; Grugeon, S.; Herrera Urbina, R.; Tekaia-Elhsissen, K.; Tarascon, J. M. *Solid State Sci.* **2002**, *4*, 665−670.

(2) (a) Lee, D. C.; Kim, J. H.; Kim, W. J.; Kang, J. H.; Moon, S. H. *Appl. Catal., A* **2003**, *244*, 83−91. (b) Oosthuizen, R. S.; Nyamori, V. O. *Platinum Met. Rev.* **2011**, *55*, 154−169. (c) Ortel, E.; Polte, J.; Bernsmeier, D.; Eckhardt, B.; Paul, B.; Bergmann, A.; Strasser, P.; Emmerling, F.; Kraehnert, R. *Appl. Catal., A* **2015**, *493*, 25−32. (d) Seth, D.; Sarkar, A.; Ng, F. T. T.; Rempel, G. L. *Chem. Eng. Sci.* **2007**, *62*, 4544−4557. (e) Silvestre-Albero, J.; Rupprechter, G.; Freund, H.-J. *Chem. Commun.* **2006**, 80−82.

(3) Guo, X.-F.; Jang, D.-Y.; Jang, H.-G.; Kim, G.-J. *Catal. Today* **2012**, *186*, 109−114.

(4) (a) Ghasemi, S.; Hosseini, S. R.; Nabipour, S.; Asen, P. *Int. J. Hydrogen Energy* **2015**, *40*, 16184−16191. (b) Darabdhara, G.; Amin, M. A.; Mersal, G. A. M.; Ahmed, E. M.; Das, M. R.; Zakaria, M. B.; Malgras, V.; Alshehri, S. M.; Yamauchi, Y.; Szunerits, S.; Boukherroub, R. *J. Mater. Chem. A* **2015**, *3*, 20254.

(5) Zheng, J.-S.; Zhang, X.-S.; Li, P.; Zhu, J.; Zhou, X.-G.; Yuan, W.-K. *Electrochem. Commun.* **2007**, *9*, 895−900.

(6) Yang, S.; Shen, C.; Lu, X.; Tong, H.; Zhu, J.; Zhang, X.; Gao, H.-j. *Electrochim. Acta* **2012**, *62*, 242−249.

(7) (a) Huang, H.; Wang, X. *J. Mater. Chem. A* **2014**, *2*, 6266−6291. (b) Frackowiak, E.; Béguin, F. *Carbon* **2001**, *39*, 937−950.

(8) (a) Hessel, V.; Hardt, S.; Löwe, H., A Multi-Faceted, Hierarchic Analysis of Chemical Micro Process Technology: Sections 1.6−1.9. In *Chemical Micro Process Engineering*; Wiley-VCH: Weinheim, Germany, 2005; pp 66−124. (b) Ortel, E.; Sokolov, S.; Zielke, C.; Lauermann, I.; Selve, S.; Weh, K.; Paul, B.; Polte, J.; Kraehnert, R. *Chem. Mater.* **2012**, *24*, 3828−3838.

(9) Feng, D.; Lv, Y.; Wu, Z.; Dou, Y.; Han, L.; Sun, Z.; Xia, Y.; Zheng, G.; Zhao, D. *J. Am. Chem. Soc.* **2011**, *133*, 15148−15156.

(10) Pennemann, H.; Dobra, M.; Wichert, M.; Kolb, G. *Chem. Eng. Technol.* **2013**, *36*, 1033−1041.

(11) Zapf, R.; Kolb, G.; Pennemann, H.; Hessel, V. *Chem. Eng. Technol.* **2006**, *29*, 1509−1512.

(12) Simsek, E.; Avci, A. K.; Önsan, Z. I. *Catal. Today* **2011**, *178*, 157−163.

(13) Schmidt, S. A.; Kumar, N.; Zhang, B.; Eränen, K.; Murzin, D. Y.; Salmi, T. *Ind. Eng. Chem. Res.* **2012**, *51*, 4545−4555.

(14) Qiu, H.; Bednarova, L.; Lee, W. Y. *Appl. Catal., A* **2006**, *314*, 200−207.

(15) Haas-Santo, K.; Fichtner, M.; Schubert, K. *Appl. Catal., A* **2001**, *220*, 79−92.

(16) Chen, H.; Bednarova, L.; Besser, R. S.; Lee, W. Y. *Appl. Catal., A* **2005**, *286*, 186−195.

(17) Ates, A.; Pfeifer, P.; Görke, O. *Chem. Ing. Tech.* **2013**, *85*, 664−672.

(18) (a) Tu, H.-C.; Wang, W.-L.; Wan, C.-C.; Wang, Y.-Y. *J. Phys. Chem. B* **2006**, *110*, 15988−15993. (b) Kocha, S. S.; Zack, J. W.; Alia, S. M.; Neyerlin, K. C.; Pivovar, B. S. *ECS Trans.* **2013**, *50*, 1475−1485. (c) Shinozaki, K.; Pivovar, B. S.; Kocha, S. S. *ECS Trans.* **2013**, *58*, 15−26.

(19) (a) Ahn, C.-Y.; Cheon, J.-Y.; Joo, S.-H.; Kim, J. *J. Power Sources* **2013**, *222*, 477−482. (b) Garsany, Y.; Ge, J.; St-Pierre, J.; Rocheleau, R.; Swider-Lyons, K. E. *J. Electrochem. Soc.* **2014**, *161*, F628−F640.

(20) Tang, J.; Liu, J.; Li, C.; Li, Y.; Tade, M. O.; Dai, S.; Yamauchi, Y. *Angew. Chem., Int. Ed.* **2015**, *54*, 588−593.

(21) Tang, J.; Liu, J.; Torad, N. L.; Kimura, T.; Yamauchi, Y. *Nano Today* **2014**, *9*, 305−323.

(22) Tang, J.; Liu, J.; Salunkhe, R. R.; Wang, T.; Yamauchi, Y. *Chem. Commun.* **2016**, *52*, 505−508.

(23) (a) Zhang, C.; Geng, Z.; Ma, J. *Microporous Mesoporous Mater.* **2013**, *170*, 287−292. (b) Kataoka, S.; Yamamoto, T.; Endo, A.; Nakaiwa, M.; Ohmori, T. *Colloids Surf., A* **2009**, *347*, 142−145. (c) Simanjuntak, F. H.; Jin, J.; Nishiyama, N.; Egashira, Y.; Ueyama, K. *Carbon* **2009**, *47*, 2531−2533.

(24) Chuenchom, L.; Kraehnert, R.; Smarsly, B. M. *Soft Matter* **2012**, *8*, 10801−10812.

(25) Liang, C.; Hong, K.; Guiochon, G. A.; Mays, J. W.; Dai, S. *Angew. Chem., Int. Ed.* **2004**, *43*, 5785−5789.

(26) Tanaka, S.; Nishiyama, N.; Egashira, Y.; Ueyama, K. *Chem. Commun.* **2005**, 2125−2127.

(27) Song, L.; Feng, D.; Fredin, N. J.; Yager, K. G.; Jones, R. L.; Wu, Q.; Zhao, D.; Vogt, B. D. *ACS Nano* **2010**, *4*, 189−198.

(28) Mitome, T.; Uchida, Y.; Egashira, Y.; Nishiyama, N. *Colloids Surf., A* **2014**, *449*, 51−56.

(29) (a) Tanaka, S.; Katayama, Y.; Tate, M. P.; Hillhouse, H. W.; Miyake, Y. *J. Mater. Chem.* **2007**, *17*, 3639−3645. (b) Liang, C.; Dai, S. *J. Am. Chem. Soc.* **2006**, *128*, 5316−5317.

(30) Kimura, T.; Emre, A. M.; Kato, K.; Hayashi, Y. *J. Mater. Chem. A* **2013**, *1*, 15135−15141.

(31) Kataoka, S.; Yamamoto, T.; Inagi, Y.; Endo, A.; Nakaiwa, M.; Ohmori, T. *Carbon* **2008**, *46*, 1358−1360.

(32) Tanaka, S.; Doi, A.; Nakatani, N.; Katayama, Y.; Miyake, Y. *Carbon* **2009**, *47*, 2688−2698.

(33) Sun, Z.; Sun, B.; Qiao, M.; Wei, J.; Yue, Q.; Wang, C.; Deng, Y.; Kaliaguine, S.; Zhao, D. *J. Am. Chem. Soc.* **2012**, *134*, 17653−17660.

(34) Ortel, E.; Hertwig, A.; Berger, D.; Esposito, P.; Rossi, A. M.; Kraehnert, R.; Hodoroaba, V.-D. *Anal. Chem.* **2016**, *88*, 7083−7090.

(35) Ruland, W.; Smarsly, B. *J. Appl. Crystallogr.* **2002**, *35*, 624−633.

(36) Crepaldi, E. L.; Soler-Illia, G. J. d. A. A.; Grosso, D.; Cagnol, F.; Ribot, F.; Sanchez, C. *J. Am. Chem. Soc.* **2003**, *125*, 9770−9786.

(37) Han, Y. F.; Kumar, D.; Sivadinarayana, C.; Goodman, D. W. *J. Catal.* **2004**, *224*, 60−68.

(38) Li, Q.; Liang, W.; Ku Shang, J. *Appl. Phys. Lett.* **2007**, *90*, 063109.

DOI: 10.1021/acscatal.6b02240
ACS Catal. 2016, 6, 8255−8263

(39) Aoki, Y.; Urita, K.; Noguchi, D.; Itoh, T.; Kanoh, H.; Ohba, T.; Yudasaka, M.; Iijima, S.; Kaneko, K. *Chem. Phys. Lett.* **2009**, *482*, 269−273.
(40) Zhao, X.; Wang, A.; Yan, J.; Sun, G.; Sun, L.; Zhang, T. *Chem. Mater.* **2010**, *22*, 5463−5473.
(41) Blackstock, J. J.; Rostami, A. A.; Nowak, A. M.; McCreery, R. L.; Freeman, M. R.; McDermott, M. T. *Anal. Chem.* **2004**, *76*, 2544−2552.
(42) (a) Bernsmeier, D.; Ortel, E.; Polte, J.; Eckhardt, B.; Nowag, S.; Haag, R.; Kraehnert, R. *J. Mater. Chem. A* **2014**, *2*, 13075−13082. (b) Yan, H.; Cheng, H.; Yi, H.; Lin, Y.; Yao, T.; Wang, C.; Li, J.; Wei, S.; Lu, J. *J. Am. Chem. Soc.* **2015**, *137*, 10484−10487.
(43) (a) Silvestre-Albero, J.; Rupprechter, G.; Freund, H.-J. *J. Catal.* **2006**, *240*, 58−65. (b) Dal Santo, V.; Gallo, A.; Naldoni, A.; Sordelli, L. *Inorg. Chim. Acta* **2012**, *380*, 216−222.
(44) (a) Wilde, M.; Fukutani, K.; Ludwig, W.; Brandt, B.; Fischer, J.-H.; Schauermann, S.; Freund, H.-J. *Angew. Chem., Int. Ed.* **2008**, *47*, 9289−9293. (b) Neyman, K. M.; Schauermann, S. *Angew. Chem., Int. Ed.* **2010**, *49*, 4743−4746. (c) Aleksandrov, H. A.; Viñes, F.; Ludwig, W.; Schauermann, S.; Neyman, K. M. *Chem. - Eur. J.* **2013**, *19*, 1335−1345.
(45) Ortel, E.; Polte, J.; Bernsmeier, D.; Eckhardt, B.; Paul, B.; Bergmann, A.; Strasser, P.; Emmerling, F.; Kraehnert, R. *Appl. Catal., A* **2015**, *493*, 25−32.
(46) Xu, B.; Fan, Y.; Zhang, Y.; Tsubaki, N. *AIChE J.* **2005**, *51*, 2068−2076.
(47) Lasia, A., Hydrogen evolution reaction. In *Handbook of Fuel Cells*; Wiley: Chichester, U.K., 2010.
(48) Pentland, N.; Bockris, J. O. M.; Sheldon, E. *J. Electrochem. Soc.* **1957**, *104*, 182−194.
(49) Bhowmik, T.; Kundu, M. K.; Barman, S. *ACS Catal.* **2016**, *6*, 1929−1941.
(50) Bai, S.; Wang, C.; Deng, M.; Gong, M.; Bai, Y.; Jiang, J.; Xiong, Y. *Angew. Chem., Int. Ed.* **2014**, *53*, 12120−12124.
(51) Cukic, T.; Kraehnert, R.; Holena, M.; Herein, D.; Linke, D.; Dingerdissen, U. *Appl. Catal., A* **2007**, *323*, 25−37.

DOI: 10.1021/acscatal.6b02240
ACS Catal. 2016, 6, 8255−8263